

# Pitted cones and domes on Mars: Observations in Acidalia Planitia and Cydonia Mensae using MOC, THEMIS, and TES data

William H. Farrand

Space Science Institute, Boulder, Colorado, USA

Lisa R. Gaddis and Laszlo Keszthelyi

Astrogeology Team, U.S. Geological Survey, Flagstaff, Arizona, USA

Received 19 May 2004; revised 3 March 2005; accepted 31 March 2005; published 17 May 2005.

[1] Domes and cones with summit pits located in Acidalia Planitia and Cydonia Mensae were studied using MOC and THEMIS images and a TES-derived thermal inertia map. North of 40.5°N latitude, the features have a dome-like morphology, and south of that latitude, the morphology is more cone-like. Layering is apparent in the summit craters of fresher looking southern cones, and asymmetric aprons were observed in some instances. Some of the northern domes also display layering in their summit craters, but asymmetric aprons were not observed. The northern domes can also display multiple summit pits or no summit pits at all and can occur in association with higher-albedo “pancake” features. The northern domes are higher in albedo but have apparent thermal inertias that are lower than the surrounding plains. The apparent thermal inertia values of the southern cones range from values comparable to the surrounding plains to slightly lower. From the TES thermal inertia map, we infer that the thermal inertia values of the pitted cones are between those of basaltic fine dust and sand, while those of the surrounding plains are closer to that of basaltic sand. While a unique interpretation of the origin of the pitted cones is not possible with the available data, we do not find compelling evidence to suggest an origin related to either basaltic volcanism or ground-ice. Instead, an origin for these features through some combination of mud volcanism and evaporite deposition around geysers and/or springs is most consistent with the observations.

**Citation:** Farrand, W. H., L. R. Gaddis, and L. Keszthelyi (2005), Pitted cones and domes on Mars: Observations in Acidalia Planitia and Cydonia Mensae using MOC, THEMIS, and TES data, *J. Geophys. Res.*, 110, E05005, doi:10.1029/2004JE002297.

## 1. Introduction

[2] The presence of small pitted cones on the northern plains of Mars was first recognized from analysis of Viking Orbiter imagery [Allen, 1979; Frey *et al.*, 1979]. Largely on the basis of crater/cone diameter ratio comparisons, these features were initially thought to be analogous to terrestrial rootless cones (pseudocraters) [Frey and Jarosewich, 1982] such as those that occur in the Lake Myvatn region of Iceland [Thorarinsson, 1953]. However, there is a disparity in size between the cones observed in the Viking imagery (mean diameter of ~542 m, this study) and the Icelandic rootless cones (mean diameter of ~50 m [Greeley and Fagents, 2001]). Smaller cones, with sizes commensurate with terrestrial rootless cones, have since been observed in Mars Orbital Camera (MOC) images of volcanic plains in Elysium Planitia and Amazonis Planitia [Lanagan *et al.*, 2001; Greeley and Fagents, 2001]. The larger pitted cones that occur in the northern plains of Acidalia Planitia and Cydonia Mensae are distinct from the smaller cones both in terms of geologic setting, size, and, in some cases, mor-

phology. Within the Acidalia and Cydonia areas studied here, there appear to be at least two classes of cones. Frey and Jarosewich [1982] also recognized differences in cone morphology, and McGill [2002] noted that more than one process could be involved in the formation of these features.

[3] Uncertainty over the nature of the pitted cones is mirrored by the ongoing debate over the nature and geologic history of the Martian northern plains themselves. Recent research has provided very different views of how the northern plains might have formed. Theories of the formation of the northern plains include their having been submerged beneath a long standing ocean [Parker *et al.*, 1989, 1993; Baker *et al.*, 1991; Head *et al.*, 1999] to their being formed by in situ alteration processes following emplacement of CO<sub>2</sub>-charged debris flows [Tanaka *et al.*, 2001]. By examining the morphology and occurrence of the pitted cones, further insights might be gained into the role that water and other volatiles might have played in shaping the northern plains as a whole. Data collected by the Mars Global Surveyor’s (MGS) MOC narrow-angle (NA) camera and Thermal Emission Spectrometer (TES) were compared with data from the Thermal Infrared Imaging System (THEMIS) on board the Mars Odyssey orbiter to study the pitted cones in the northern plains of Mars. The

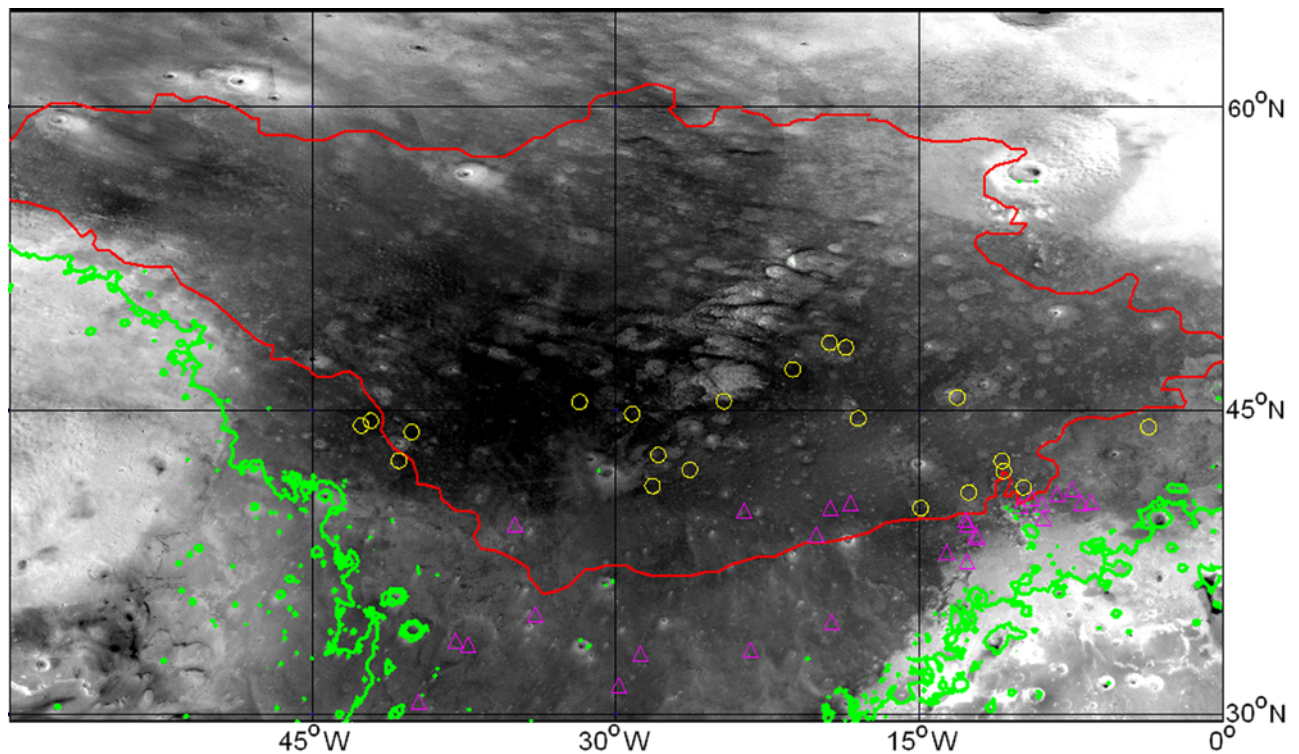


**Figure 1.** Context image of Acidalia Planitia region using a MOC wide-angle mosaic as background. The green boundary follows the MOLA-determined  $-3760$  m elevation contour, which approximates the “Contact 2” or Deuteronilus putative shoreline [Parker *et al.*, 1989]. The red line outlines the outer boundary of the Hvm, Hvr, and Hvg units of the Vastitas Borealis Formation as it occurs in this region [Scott and Tanaka, 1986]. Occurrences of northern domes examined in this study are plotted as yellow circles, and southern cones are plotted as magenta triangles.

geomorphology, mineralogy, and thermophysical properties of the cones, as well as their relation to the surrounding plains were examined using these data. These observations were then used to constrain the most likely formation processes for these pitted cones. In the following, we place the cones and domes in their geologic setting, detail the data sets used, describe the new observations made, and then systematically investigate a wide range of plausible formation mechanisms to reach our final conclusions.

## 2. Geologic Setting

[4] We focus our attention on the greater Acidalia Planitia (centered approximately at  $44^{\circ}\text{N}$ ,  $21^{\circ}\text{W}$ ) region of the vast northern plains of Mars. We include part of the Cydonia region (centered approximately at  $34^{\circ}\text{N}$ ,  $9^{\circ}\text{W}$ ) immediately to the east of Acialia. This study area has abundant occurrences of pitted cones. Acidalia is a classical dark region in the northern lowlands of Mars. Recently, on the basis of the analysis of TES data, it was designated as the type locale for the “surface type 2” spectral class which has been interpreted as andesitic in composition while the “surface type 1” spectral class is interpreted as basaltic [Bandfield *et al.*, 2000]. Several outflow channels, including Ares, Tiu and Kasei Valles, emptied into the Acidalia basin. If the hypothesized northern ocean existed, much of Acidalia would have been submerged. For example, Figure 1 shows that the  $-3760$  m elevation contour, which closely approximates the “Contact 2” [Parker *et al.*, 1989] or

“Deuteronilus” [Clifford and Parker, 2001] putative shoreline, encompasses most of Acidalia and Cydonia. The portion of Cydonia examined in this study extends from Acidalia on the west to  $0^{\circ}$  longitude and from approximately  $30^{\circ}\text{N}$  to  $40^{\circ}\text{N}$  in latitude. While parts of Cydonia rise above the  $-3760$  m contour, all of the pitted cones and domes examined in this study occurred below the  $-3760$  contour (see Figure 1).

[5] Much of northern Acidalia has been mapped as being covered by the Vastitas Borealis Formation (VBF) (the outer boundary of which is denoted by the red line in Figure 1). There are competing hypotheses for the origin of the VBF and the shaping of the northern plains. The mottled and knobby members of the VBF were originally interpreted as being volcanic in origin [Scott and Tanaka, 1986]. More recent discussions of the nature of the VBF dispute the role of volcanism in its formation. The VBF surface has been described variously as the former ocean floor of a standing northern ocean [Parker *et al.*, 1989, 1993; Baker *et al.*, 1991], as a clastic sedimentary unit dropped from suspension from a short-lived ocean produced by the outflow channels to the south [Kreslavsky and Head, 2002], and as the product of in situ reworking/alteration of preexisting materials by permafrost-related processes [Tanaka *et al.*, 2003]. A sedimentary origin had previously been posited for the polygonally fractured terrain within the VBF by McGill and Hills [1992] and a “mud ocean” covering the northern plains was posited by Jöns [1985, 1986]. While there are numerous pitted cones within the VBF, they also occur

beyond its boundaries. This study addresses pitted cones within both the VBF and parts of Cydonia Mensae that lie outside of the mapped boundaries of the VBF. Depending on how boundaries are drawn, the western portion of Cydonia includes the AHvh unit, or the hummocky member of the VBF, of *Tanaka et al.* [2003]; Hb2, the Hesperian boundary plains unit of *Tanaka et al.* [2003]; and Hnu undivided Noachian and Hesperian aged material.

[6] This evolution in thinking about the nature of the VBF and the northern plains of Mars leads to a corresponding range in plausible hypotheses for the formation of the pitted cones and domes, including purely volcanic cinder cones, phreatomagmatic constructs, mud volcanoes, and pingos formed by the freezing of mobile groundwater. These various origin hypotheses have implications for the nature of the northern plains in general and that of the VBF in particular. Pitted cone origin hypotheses that require the action of water would also suggest that water could also have played a major role in the formation of the VBF. If we can eliminate some of the origin hypotheses from the large list of possible processes that could have formed the pitted cones, we may be able to place additional constraints on the nature and origin of the northern plains.

### 3. Data and Data Analysis

[7] Data from several Mars Global Surveyor (MGS) and Mars Odyssey (MO) instruments were used in this study. Detailed morphologic assessments and size measurements of the cones were made using MOC NA camera and THEMIS Visible (Vis) camera images ingested into the USGS ISIS software [*Eliason, 1997; Gaddis et al., 1997; Torson and Becker, 1997*]. The MOC images have spatial resolutions ranging from 1.5 to 6 m/pixel. The nominal spatial resolution of THEMIS Vis imagery is 19 m/pixel. These high-resolution images, along with 100-m-pixel, day and night, single-band THEMIS Mid-Wave Infrared (MWIR) images, were geometrically registered to a common areocentric coordinate system using the ISIS software and were overlain on several different image basemaps using Geographic Information System (GIS) software. USGS scripts [*Hare and Tanaka, 2004*] were used to aid in taking the data from the ISIS processing environment to the GIS. The images were overlaid on multiple coregistered data sets, including the 128 pixels per degree gridded topography from the Mars Orbiting Laser Altimeter (MOLA), a MOC wide-angle camera mosaic, a 20 pixel per degree thermal inertia map derived from the Thermal Emission Spectrometer (TES) [*Mellon et al., 2002*], and 4 pixel per degree mineral abundance maps derived from TES [*Bandfield, 2003*]. The THEMIS day/night image pairs were used in conjunction with the TES thermal inertia map [*Mellon et al., 2002*] to extract information on thermophysical properties.

[8] The THEMIS data were obtained from the Planetary Data System (PDS) in the form of calibrated at-sensor radiance. The individual channels are not inherently coregistered. To achieve coregistration, ISIS software was used to register the bands to each other and to georegister them so that they could be coregistered with, and compared with, the other GIS image bases.

[9] Qualitative examination of multispectral properties was conducted using both the THEMIS Vis and MWIR cameras [*Christensen et al., 2004*]. THEMIS has 10 MWIR bands; 9 of these bands are useful for surface studies. These are bands 1–9, centered at 6.78, 6.78, 7.93, 8.56, 9.35, 10.21, 11.04, 11.79, and 12.57  $\mu\text{m}$ , respectively. For the GIS mosaics assembled for this study, we used band 8 (11.79  $\mu\text{m}$ ) for the daytime scenes and band 9 (12.57  $\mu\text{m}$ ) for the nighttime scenes. To look for relative color differences in the THEMIS MWIR data, a smaller number of component scenes from these mosaics were examined using the nine THEMIS bands for surface analysis. Several standard multispectral processing approaches, including band ratios, principal components analysis, and decorrelation stretches [*Gillespie et al., 1986*] were applied to these scenes. The THEMIS Vis camera has 5 bands in the visible to near infrared (VNIR) (band centers at 0.42, 0.54, 0.65, 0.75, and 0.86  $\mu\text{m}$ ). In all THEMIS Vis images examined, the fifth band was unusable due to an unacceptably low SNR.

[10] The THEMIS MWIR data provide important information on thermophysical properties of the surfaces imaged and work is ongoing to derive calibrated THEMIS thermal inertia data [*Ferguson and Christensen, 2003*]. However, given the current absence of a standardized method of determining thermal inertia from THEMIS data, we improvised an approach for deriving thermal inertia from nighttime THEMIS data. This involved a process of overlaying the night 100-m-pixel THEMIS data on a 3-km-pixel map of thermal inertia derived from TES [*Mellon et al., 2002*]. By matching the relative gray level of homogenous plains regions in the night THEMIS images to the underlying thermal inertia image, estimates were derived for the thermal inertia of the background plains. This approach is illustrated in Figure 2. For the cones, a range of approximate values were derived by noting a region where the THEMIS radiance values were the same as a broader patch of plains material that then could be matched to the lower spatial resolution TES thermal inertia map. Thermal inertia values derived via this methodology are noted in Table 2.

[11] TES data were used in this study in the form of the aforementioned thermal inertia map derived from TES data [*Mellon et al., 2002*] and in the form of 4 pixel per degree mineral abundance maps derived by *Bandfield* [2002]. As was noted earlier, *Bandfield et al.* [2000] referenced Acidalia as being the type region for the second major dark region surface type. The first surface type has an emittance spectrum similar to a terrestrial flood basalt and is typified by spectra of Syrtis Major. The “surface type 2” material, typified by the Acidalia dark region, has an emittance spectrum that is well modeled by a more andestic composition [*Bandfield et al., 2000*] although weathered basalt has been suggested as a viable alternative interpretation [e.g., *Wyatt and McSween, 2002*]. The analysis of *Bandfield et al.* [2000] was performed using atmospherically corrected emittance spectra binned into one pixel per degree maps. Mineral maps were obtained through application of a linear deconvolution analysis that modeled TES emittance spectra as linear combinations of laboratory measured emittance of mineral samples after the approach of *Ramsey and Christensen* [1998]. A later version of this

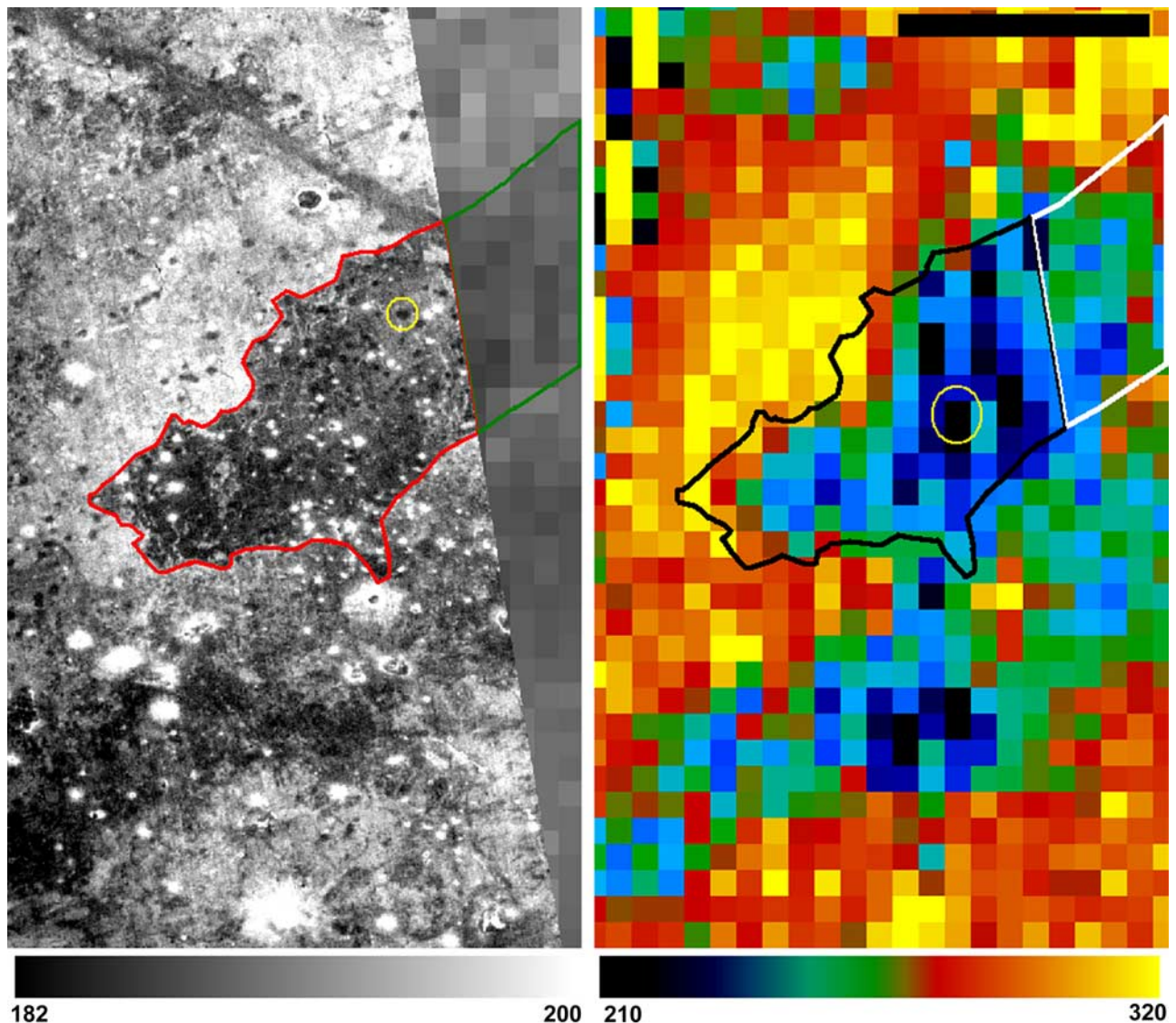


**Figure 2.** Example of two ways in which gray levels in units in nighttime THEMIS images were matched to corresponding values in the TES thermal inertia image. Left image shows a subsection of THEMIS scene I04501005 overlaid on the TES thermal inertia image. Scale bar at bottom shows brightness temperature values (in degrees K) for the THEMIS scene. Right image shows pseudocolored version of TES thermal inertia image with color ramp bar at bottom for TI values in  $\text{J m}^{-2} \text{s}^{-1/2} \text{K}^{-1}$ . Direct extractions of thermal inertia were possible for large units such as the area outlined in green on the left and white on the right. Estimates of thermal inertia for smaller features such as the pitted cone circled in yellow on the left were derived by matching to broader plains units with comparable digital numbers, and these were related to a TES thermal inertia pixel such as the one circled in yellow on the right. Scale bar in the upper right is 20 km in length.

analysis produced the 4 pixel per degree mineral abundance maps [Bandfield, 2002] used in this study.

#### 4. Observations

[12] At least two major morphologic types of “pitted cones” are recognized in this study area (Figure 1). Frey and Jarosewich [1982] noted, and this study confirmed, that “cones” occurring on more northerly fractured plains units (regions split by giant polygons) tend to be larger (wider basal diameter) than cones occurring on smooth plains units in the south. The larger fractured-plains “cones” have a more

rounded, mound- to dome-shaped morphology (Figure 3a). For this latter group, summit craters might be lacking, can be irregular in shape, or can have multiple pits on the summit and flanks (Figure 3b). We prefer the term “domes” for these features. These pitted domes can also occur in association with irregularly shaped splotches that are high in albedo relative to the dark Acidalia plains (Figure 3c). There are also circular “pancakes” of higher-albedo material, apparently filling depressions (Figure 3d). As shown in Figure 1, these pitted domes tend to occur north of  $40^{\circ}30'N$ . The cones south of this latitude have a more definitive cone-like morphology (smaller crater/base diameter ratio than the northern

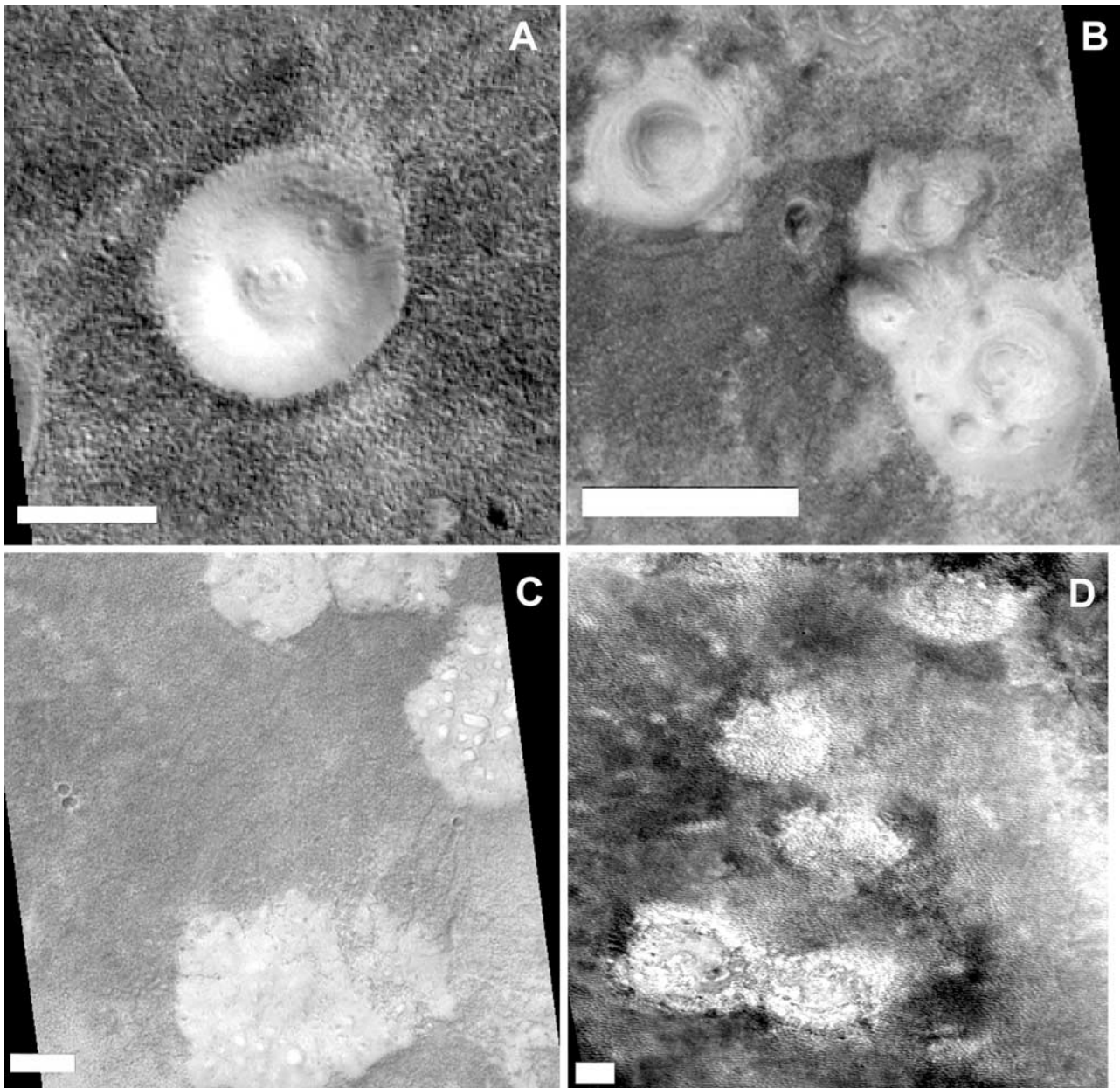


**Figure 3.** MOC NA images of northern domes. North is to the top in all images, and each scale bar represents 400 m of length. (a) Representative northern dome occurring in MOC NA image M03-06847. Note relative bright albedo as compared to surrounding plains. Subsection is centered at  $42.51^{\circ}\text{N}$ ,  $40.72^{\circ}\text{W}$ . Solar azimuth of this image is  $322.27^{\circ}$ . (b) Northern dome displaying multiple summit pits. Feature occurs in MOC NA image E21-00496. Subsection is centered at  $42.31^{\circ}\text{N}$ ,  $26.38^{\circ}\text{W}$ . Solar azimuth of this image is  $340.87^{\circ}$ . (c) Example of bright splotches on Acidalia dark plains. From MOC NA image M21-01816. Subsection is centered at  $41.73^{\circ}\text{N}$ ,  $26.81^{\circ}\text{W}$ . Solar azimuth of this image is  $340.29^{\circ}$ . (d) Example of recessed “pancake” bright circular features in subset of MOC NA image E05-01293. Subsection is centered at  $49.35^{\circ}\text{N}$ ,  $18.46^{\circ}\text{W}$ . Solar azimuth of this image is  $319.5^{\circ}$ .

domes), but can be found in more eroded forms (Figure 4a). Some of these “smooth plains” cones can have aprons that are elongated in a single direction (Figure 4b). The cones in Figure 4b also clearly have concentric dark and light layers within their summit craters. The “southern cones” often occur in clusters, while the “northern domes” tend to have more isolated occurrences. Occurrences of pitted cone clusters were noted concentrated within the rim of subdued crater forms (dubbed “stealth craters” by *Kreslavsky and Head*

[2002]). A notable example is the large stealth crater in southwestern Acidalia centered at approximately  $34.4^{\circ}\text{N}$ ,  $37.2^{\circ}\text{W}$ . Figure 4a is an example of one of the degraded cones that are clustered inside this crater. Cones have also been noted to occur in linear or arc-shaped chains; an example of such an occurrence is the domes shown in Figure 5. In THEMIS Vis images examined in this study, the examples of these chains that were observed are relatively short in length, on the order of 4 km or less

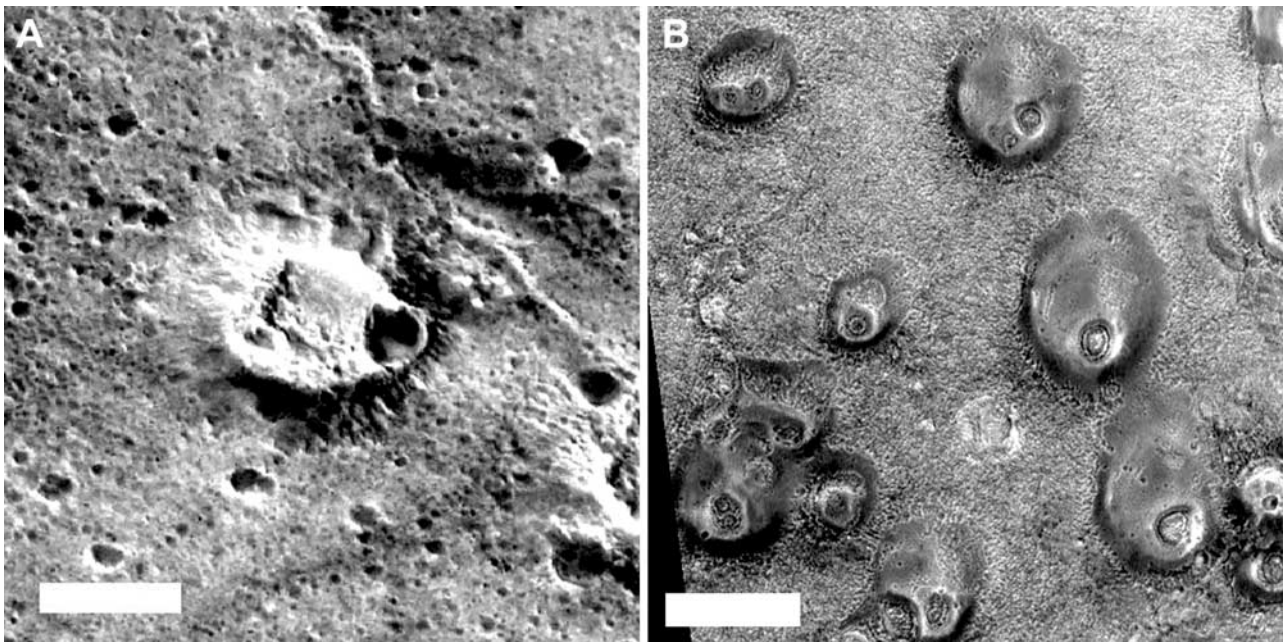


**Figure 4.** (a) Example of degraded southern cone. Feature occurs in MOC NA image M03-00774. Subsection is centered on  $34.54^{\circ}\text{N}$ ,  $36.34^{\circ}\text{W}$ . Scale bar is 400 m. North is to the top of the image. Solar azimuth of this image is  $333.21^{\circ}$ . (b) Southern cones with elongated ejecta aprons. Subsection taken from MOC NA image E20-00551. Subsection is centered on  $37.89^{\circ}\text{N}$ ,  $12.65^{\circ}\text{W}$ . Scale bar is 400 m. North is to the top of the image. Solar azimuth of this image is  $343.01^{\circ}$ .

and appear unrelated to identified surface features. While *Frey and Jarosewich* [1982] used the nomenclature of “fractured plains” and “smooth plains” cones, here we refer to these groups, respectively, as “northern domes” and “southern cones”.

[13] Size information was derived for 180 cones in Acidalia and Cydonia examined in MOC NA and THEMIS visible camera images. The derived crater and basal diameters and the crater/base diameter ratios are shown in Table 1. The diameter of the crater is defined as the rim-to-rim distance and the basal diameter is defined as the distance between the most apparent breaks in slope between the flanks of the feature and the plains on opposite sides of the cone/dome. Heights for three cones were derived from three MOLA altimeter tracks over cones seen in MOC NA pairs in the Acidalia and Cydonia regions. The derived heights must be considered minimum values since the MOLA spot might have been offset from the cone summit and also due to the fact that the MOLA spot size is nominally 180 m in diameter. The range of cone heights from these tracks is 36 to 65 m. These results are in accord with values for the height of cones in Isidis Planitia obtained by *Fagents et al.* [2002]. For the few instances where we did find MOLA tracks going over cones or domes in MOC NA images, we calculated slopes and found them in the range of 6 to 11 degrees; however, given the sparse MOLA sampling for such small-scale features and uncertainties inherent in the location of MOLA footprints we view these values as highly uncertain and possibly unrepresentative. For cones in Isidis Planitia, *Fagents et al.* [2002], again using sparse MOLA track coverage, estimated that the slopes of those features could be no steeper than 50 degrees.

[14] Using the processing approaches listed previously, it was determined that in the multispectral MWIR data, there

were no color differences between the pitted cones and the background that were any greater than color variations in the background plains material. In the Vis bands of THEMIS and in MOC NA camera images, there were, again, no significant color differences; however, albedo differences between pitted cones in Acidalia and the dark background plains were noted (for example, Figure 3a) with cones in Acidalia generally having a higher radiance factor (I/F) than the background. The radiance factors of cones in Cydonia were comparable to the background plains or sometimes slightly lower. Calibrated I/F values for cones and background plains from select MOC NA images processed using the ISIS software are shown in Table 2. These broadband I/F values were extracted directly from the ISIS processed images [*Becker et al.*, 2004]. The data output from ISIS processing are in the form of exo-atmospheric I/F. No atmospheric correction was applied to the data since the intent of the analysis was to provide an assessment of the relative brightness differences between the pitted cones and the surrounding plains.

[15] Even without a conversion to units of thermal inertia, nighttime THEMIS images can be used to estimate relative trends in thermal inertia. Figure 5 shows a scattered distribution of northern domes within the same region in Acidalia as covered by both daytime and nighttime THEMIS images. Arrows in Figure 5 point to examples of these northern pitted domes. It can be seen that they are bright relative to the background in the daytime THEMIS scene and dark relative to the background in the nighttime THEMIS scene. Materials with relatively high thermal inertia values tend to be dark in daytime and bright in nighttime THEMIS images. The reverse is true for materials that are relatively low in thermal inertia. Within a given nighttime scene, bright and dark areas represent *relative* differences in thermal inertia; a dark region in a

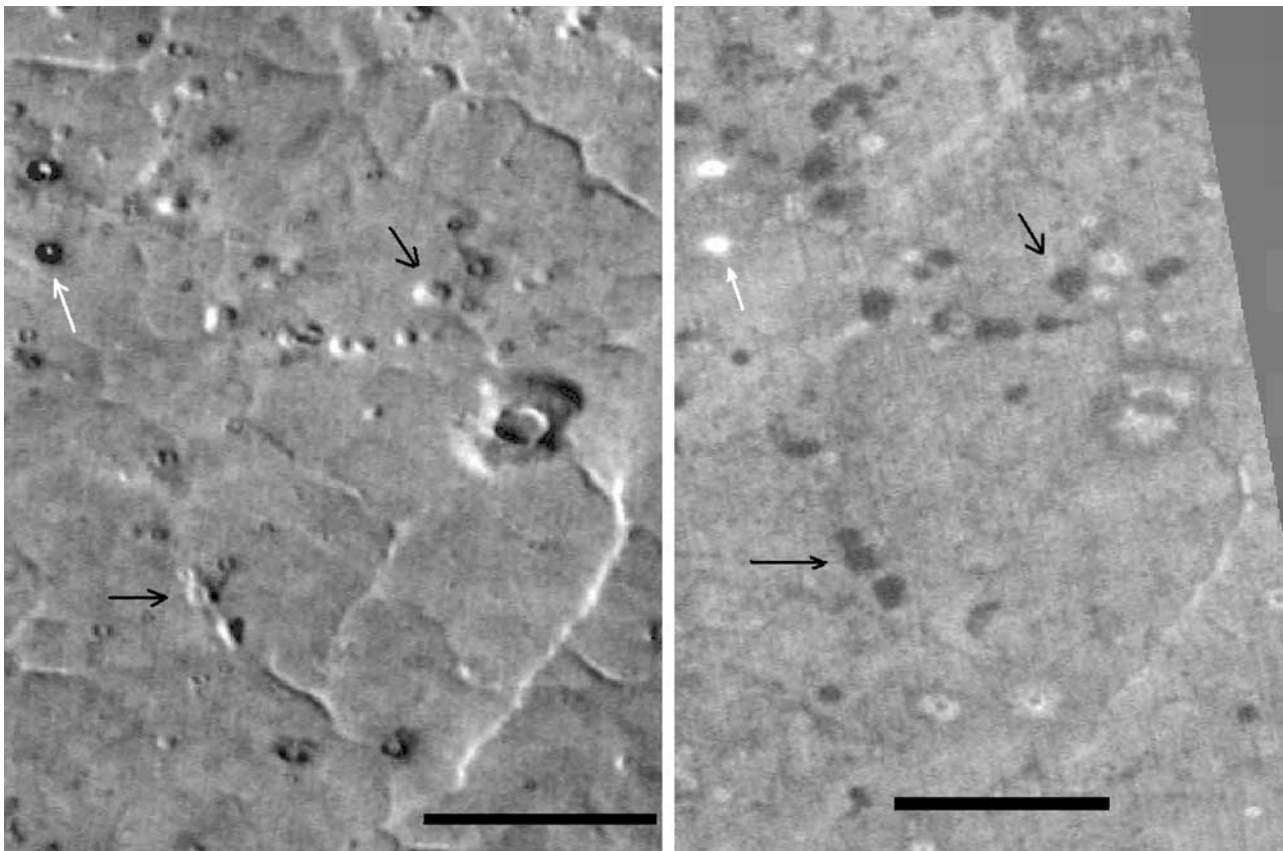


**Figure 5.** (left) Daytime (I03271002) and (right) nighttime (I04638003) THEMIS MWIR images over a portion of Acidalia Planitia. Solar illumination is from the lower left in the daytime image. White arrow points to a pair of fresh craters that are dark in the daytime and bright in the nighttime THEMIS data. Black arrows point to representative examples of northern domes which are bright to neutral in the daytime THEMIS image but dark in the nighttime THEMIS image. Note that some of these cones are aligned in chains. The black scale bar is 10 km long. North is to the top in both images.

high thermal inertia plains unit in a nighttime THEMIS scene can still have a comparatively high value of thermal inertia.

[16] In contrast to the relative difficulty in extracting thermal inertia from THEMIS data, the THEMIS radiance data can be readily converted to brightness temperature. Brightness temperatures of the pitted cones and background materials were directly extracted from THEMIS brightness temperature images provided to the PDS (actual brightness temperature values were determined using scaling factors provided in the PDS headers). Average brightness temperatures for southern cones in Acidalia and in Cydonia (over the solar longitude ( $L_s$ ) range  $142^\circ$  to  $148^\circ$ ) and northern domes in Acidalia (over the  $L_s$  range  $110^\circ$  to  $124^\circ$ ) are shown in Table 2. Not all occurrences of pitted cones are thermally distinct from their background. Some occurrences of southern cones in Acidalia were indistinguishable to nearly indistinguishable from the background in the nighttime THEMIS images (Figure 6). In all of the examined imagery, the northern domes were distinct from the background. Also, the relatively flat “pancake” features noted above and visible-wavelength bright splotches are cold relative to the background in the nighttime THEMIS imagery (Figure 7).

[17] The estimated thermal inertia of the northern domes is in the range of 210 to 240  $\text{J m}^{-2} \text{s}^{-1/2} \text{K}^{-1}$  and that of the

southern cones is in the range of 190 to 210  $\text{J m}^{-2} \text{s}^{-1/2} \text{K}^{-1}$ . These values are between the thermal inertia of basaltic fine to coarse sand (155 and 374  $\text{J m}^{-2} \text{s}^{-1/2} \text{K}^{-1}$ ) [Mellon, 2001]. The thermal inertias of the fractured plains are closer to the basaltic sand value and that of the smooth plains are in the same approximate range as that of the pitted cones. These values explain why the southern cones sometimes blend in with the background in the nighttime THEMIS images.

[18] The TES-derived 4 pixel per degree mineral abundance maps of *Bandfield* [2003] indicated only that the composition of the study area is consistent with the “surface type 2” spectral class. Analysis of these maps did not reveal any variations in composition that could be associated specifically with the pitted cones. Earlier work by both *Farrand and Gaddis* [2003a] and *Bandfield* [2002] indicated

**Table 1.** Sizes of Southern Cones and Northern Domes

Features	Basal Diameter, m		Crater Diameter, m		Crater/Base	
	Mean	Std. Dev.	Mean	Std. Dev.	Mean	Std. Dev.
Southern cones	455	166	232	80	0.513	0.072
Northern domes	774	197	415	98	0.544	0.092

**Table 2.** Broadband I/F, Brightness Temperature, and Relative Thermal Inertia of Pitted Cones and Background Plains<sup>a</sup>

Region	Cones/Domes		Plains	
	Mean	Std. Dev.	Mean	Std. Dev.
<i>MOC NA I/F</i>				
Southern cones	0.109	0.0018	0.109	0.0027
Northern domes	0.110	0.0034	0.098	0.0029
<i>Brightness Temperature, K</i>				
Southern cones	178.5	5.7	184.85	10.7
Northern domes	189.1	2.1	196.08	3.2
<i>Thermal Inertia, <math>J m^{-2} s^{-1/2} K^{-1}</math></i>				
Southern cones	210 ± 13 to 240 ± 14		235.5	7.5
Northern domes	190 ± 11 to 210 ± 13		298.0	9.9

<sup>a</sup>Standard deviations of I/F and brightness temperature values are standard deviations of the mean for the pixels averaged together to obtain those values and do not include uncertainties inherent in the calibration to I/F or brightness temperature. Standard deviations of thermal inertia of plains are standard deviations of the mean for the pixels averaged together to obtain those values. A range of values is provided for thermal inertias of pitted cones and domes given that the values were obtained by indirect comparisons. A plus/minus value is given for the lower and upper bounds based on the approximately 6% uncertainty in the TES thermal inertia map (M. T. Mellon, personal communication).

a high fraction of basaltic glass in Acidalia. This observation could have significance since basaltic glass is often associated with ash from explosive volcanic activity and thus could support volcanic origins for the pitted cones. We note, however, that linear deconvolution [Ramsey and Christensen, 1998] of thermal infrared data is nonunique. For example, while the “surface type 2” spectral unit was initially interpreted as being andesitic in composition, it has been reinterpreted as an altered basalt [Wyatt and McSween, 2002] with clays accounting for the spectral features that were attributed to glass in the Bandfield et al. [2000] interpretation.

## 5. Discussion

[19] A variety of origins have been suggested for the cones and domes in Acidalia and Cydonia, including those related to volcanic, ground-ice, and sedimentary processes. Suggested terrestrial analogs for the northern plains cones and domes have included cinder cones [Wood, 1979], rootless cones [Frey and Jarosewich, 1982], pingos [Lucchitta, 1981; Farrand and Gaddis,

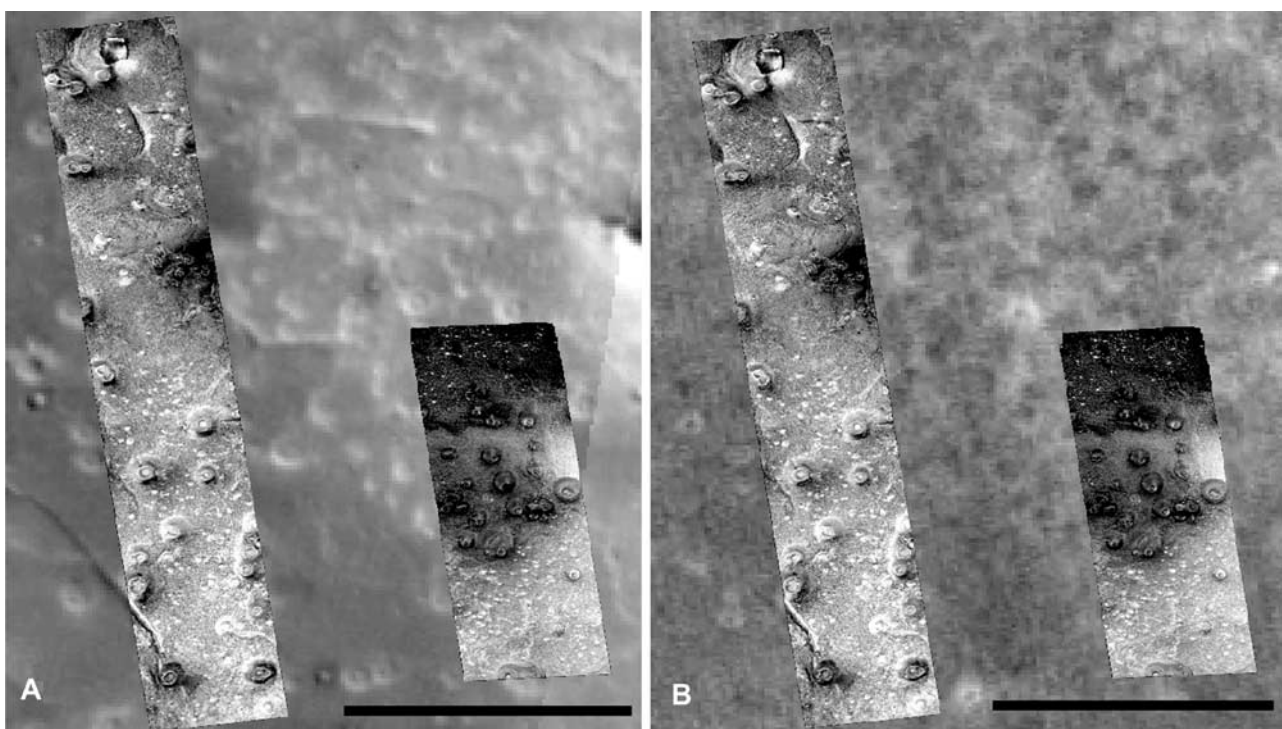


**Figure 6.** (a) MOC NA images (left) E15-01186 and (right) E20-00551 overlaid on daytime THEMIS scenes I01798002 and I01436005 (exposed in lower right). Solar illumination is from the southwest in the daytime THEMIS scenes and from the west-northwest in the MOC scenes. Note that dark plains unit in upper portion of E20-00551 is bright in daytime THEMIS scene, indicating lower thermal inertia relative to the surrounding plains. Note also that southward (Sun-facing) slopes of pitted cones are bright relative to the background. The cones are of sufficient size and contrast to be distinguished. These images are located near 37.9°N, 12.9°W. Scale bar is 8 km long. North is to the top of the image. (b) Approximately the same region as in Figure 6a with the two MOC scenes overlaid on nighttime THEMIS scene I05437014. While the spatial resolution of this THEMIS scene is comparable to the daytime scene in Figure 6a, the contrast of the pitted cones against the background is very low, indicating comparable thermal inertias. The exception is in the relatively low thermal inertia plains unit in the upper right-hand portion of the image, where the cones are darker than the background (i.e., relatively low in thermal inertia relative to the plains). Scale bar is 8 km long. North is to the top of the image.

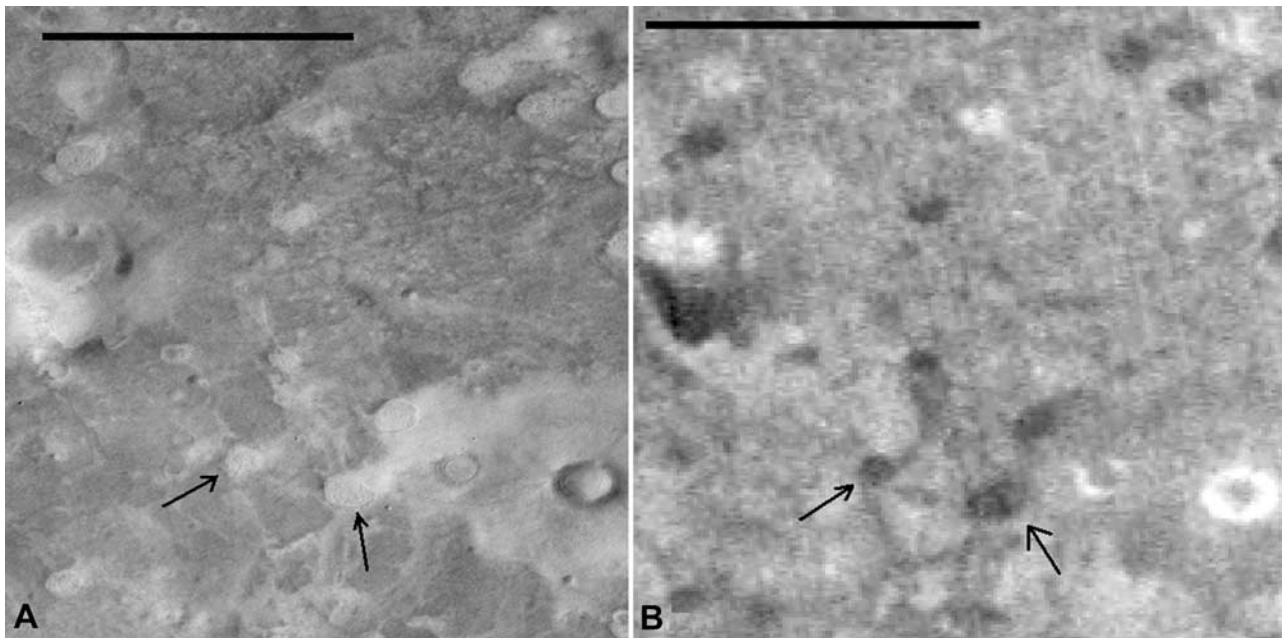


**Figure 7.** (a) Relatively flat “pancake” features filling apparent depressions in the northern plains. Arrows point to lower two “pancakes” of a set of four. Subsection of THEMIS Vis scene V04632009. Scale bar in upper left is 10 km long. The scene is centered at 48.4°N, 19.4°W. (b) Subsection of nighttime THEMIS scene I05562016 covering same area as the Vis THEMIS scene in Figure 7a. Arrows point to the same two “pancake” features, which can be seen to be dark relative to the background. Scale bar in upper left is 10 km long.

2003b], and mud volcanoes [Tanaka, 1997; Tanaka *et al.*, 2003]. Crumpler [2003] notes that spring deposits can form features similar in morphology to the pitted cones of this study.

[20] We note that there is no reason a single formation mechanism is required to explain all the cones and domes. The two groups of pitted cones are distinct not only in terms of morphology and size, but also in terms of their geographic distribution. The northern domes occur predominantly north of 40.5°N latitude and southern cones occur predominantly south of that latitude. The difference in morphology of the northern domes from the southern cones requires some associated change in formative process. Such a change could indicate either two different formation processes for the northern and southern cones or a single process with a change in some parameter (for example, amount of water included during a hydrovolcanic or mud volcano eruption). We now examine each of the proposed origins for the cones and domes of the northern plains in turn.

### 5.1. Cinder Cones

[21] Cinder cones are formed by (typically basaltic) lava fountaining from a point source in the ground. While the general size and shape of many of the southern pitted cones are similar to those of terrestrial cinder cones, there are several reasons to reject this hypothesis. First, cinder cones on Mars are expected to have a lower aspect ratio because, in Mars’ lower gravity and thinner atmosphere, ash and cinders are expected to travel further from the vent on Mars than they do on Earth [Wilson and Head, 1983]. Second, fields of cinder cones are usually associated with lava flows.

There are no obvious lava flows around the cones and domes in the Acidalia region. Third, cinder cone materials would be expected to have optical and thermal properties broadly similar to basaltic sand [Zimelman, 1986; Keszthelyi, 1994]. While the thermal properties are compatible with cinder, the cones and domes we observed are distinctly brighter than the basaltic sands in Acidalia. Moreover, the southern cones and northern domes have mean I/F values of 0.109 and 0.110 respectively, while basaltic ash, in the MOC NA images, should have a radiance factor of approximately 0.075 (value measured by Geissler *et al.* [1990] for exo-atmospheric I/F of putative basaltic ash in Valles Marineris). Finally, while having similarities to the southern cones, cinder cones are a poor morphologic analog to the northern domes.

### 5.2. Rootless Cones

[22] Rootless cones (also called pseudocraters) are formed by explosions that result from a lava flow advancing over a wet substrate. Rootless cones on Earth are typically tens of meters in diameter, but, on Mars, could have diameters similar to the cones and domes we have observed [Greeley and Fagents, 2001; Fagents *et al.*, 2002]. Rootless cones can form in chains [Bruno *et al.*, 2004], although the length and number of such chains observed for the cones and domes of Cydonia and Acidalia appears smaller than was observed in the terrestrial examples presented by Bruno *et al.* [2004]. There are two reasons why we do not favor a rootless cone origin for these features. First, they do not obviously sit on lava flows. In other locations on Mars, the interpretation of cones as rootless cones has depended on their superposition on recognizable lava surfaces [Lanagan

*et al.*, 2001; *Greeley and Fagents*, 2001]. Second, the spatter and other pyroclasts associated with rootless cones are generally quite dense. This is because the lava that is thrown out of a rootless cone has been largely degassed during flow on the surface [*Morrissey and Thordarson*, 1991]. However, the thermal inertias we observe for the cones and domes on Mars are much lower than expected for dense spatter. *Morrissey and Thordarson* [1991] note that while sediments are incorporated into Icelandic rootless cones, they are generally incorporated during the early stages of cone formation (e.g., they would be found closer to the core of the cone than to the exterior) thus it seems unlikely that there could be fine-grained sediments, associated with the eruption, that blanket the cones and reduce the apparent thermal inertia of these features. Thus, primarily on the basis of the lack of apparent lava flow features and the evidence provided by the apparent thermal inertia of these features, we conclude that rootless cones are an unlikely explanation for the cones and domes observed in Acidalia and Cydonia.

### 5.3. Phreatomagmatic Tuff Cones

[23] Tuff cones and rings form when ascending magma interacts explosively with standing water or groundwater. Tuff cones and tuff rings on Earth usually have diameters similar to the southern cones (see Table 3), but tuff rings usually have very shallow topographic expressions that are generally unlike the Martian cones we have examined. Tuff cones are primarily composed of fine-grained (ash-sized) particles and, on Earth, typically form when an eruption penetrates a shallow standing body of water [e.g., *Wohletz and Sheridan*, 1983]. Tuff cones can form without associated lava flows, making them a better candidate for explaining the Martian cones than either cinder cones or rootless cones. However, there are problems with trying to explain the observed Martian pitted cones as being tuff cones. Terrestrial tuff cones generally have asymmetric rims caused by prevailing winds moving the erupting ash preferentially in the downwind direction. While there are examples of asymmetric rims (e.g., Figure 4b) among the observed cones, in the example of the cones in Figure 4b, the elongation of the rims is in the downslope direction (from the south to the north end of MOC NA image E20-00551, a distance of 10 km, there is a drop of 56 m, a local slope of approximately 0.3 degrees, and in the nearby scene E15-01186, which also has pitted cones with elongated rims, the slope from the south to the north end of the scene is 0.4 degrees). This is more suggestive of some sort of flow process in the downhill direction (such as the effusion of muds or evaporation of chemical-laden waters, as discussed in the considerations of the final two origin processes) rather than having winds coincident with topographic gradients. Another issue is that the low thermal inertia of the Martian cones is more consistent with the presence of an unconsolidated carapace of ash than with an indurated tuff. In terrestrial tuff cone eruptions, the final ash ejected in the tuff cone forming eruption can form a carapace of unconsolidated ash. In the presence of eolian erosion, this carapace is expected to be rapidly removed, exposing more indurated, palagonitized layers within the cone. Given that we, and other researchers [e.g., *Geissler*, 2005], have noted significant eolian activity on the Acidalia plains, we find it

**Table 3.** Sizes of Potential Terrestrial Analogs to Pitted Cones<sup>a</sup>

Feature	Basal Diameter (Mean), m	Crater/Base (Mean)
Cinder cones	800 (1)	0.4 (1)
Rootless cones	80 (2)	0.47 (2)
Tuff cones	1900 (3)	0.49 (3)
Tuff rings	1900 (3)	0.56 (3)
Pingos	200 (4)	0.55 – 0.7 (1)
Mud volcanoes	4000 (5)	0.14 (5)
Spring deposits	200 (6)	0.47 (6)

<sup>a</sup>References for dimensions: 1, *Wood* [1979]; 2, *Frey and Jarosewich* [1982]; 3, *Pike and Clow* [1981] (these authors grouped tuff rings and tuff cones together; these features have been separated here on the basis of their table of features); 4, *Gurney* [1998]; 5, *Kholodov* [2002] (figures from his descriptions of cone shaped mud volcanoes in Azerbaijan; many mud volcanoes described by Kholodov have different dimensions); 6, *Roberts and Mitchell* [1987] (measurements averaged from examples cited in paper).

challenging to reconcile the thermal inertia measurements with a tuff cone origin for these features. However, we cannot discount the possibility that the exposed surface has undergone some level of alteration, perhaps leaving a porous exterior with a relatively low thermal inertia. Some level of alteration would also help to account for the increased albedo of the cones relative to the surrounding plains since the process of alteration of basaltic ash, for example, palagonitization, acts to increase the albedo of such material [*Farrand and Singer*, 1992]. The presence of significant numbers of tuff cones, formed of basaltic ash is also consistent with the TES deconvolution results noted above that indicate relatively high amounts of basaltic ash in Acidalia. We posit that, in the case of the southern cones, morphology and other observations surrounding these features are not necessarily inconsistent with an origin as tuff cones although we stress that on the basis of the available evidence this is not one of our preferred origin processes.

### 5.4. Pingos

[24] Pingos are domical structures formed by migration and freezing of groundwater. When the ice in the core of a pingo sublimates, it can leave a pitted “pingo scar” [*DeGans*, 1988]. Pingos on Earth have diameters similar to the cones and domes in the Acidalia, but are usually not as tall. For example, *Pissart* [1988] notes that 85% of terrestrial pingos are 20 m or less in height; not as tall as the 36 to 65 m minimum heights of pitted cones estimated from MOLA profiles. *Mackay* [1973, 1998] notes that pingo growth is generally accompanied by radial extension cracks. Such cracks have not been noted in any of the observed Acidalia or Cydonia pitted cones. The central collapse pits in pingos can also result in the growth of these radial cracks to form “star shaped” collapse pits [*Mackay*, 1973, 1998] that are unlike the generally symmetrical summit craters of the pitted cones. Pingo scars which have completely lost their ice cores can have more symmetrical summit pits although evidence of the preexisting radial fractures is often still discernable. Furthermore, the surfaces of pingos are composed of the same materials as their surroundings. The distinct albedo and variable thermal properties of the cones and domes is therefore not consistent with the pingo hypothesis. In summary, we find the observed character-

istics of the cones and domes to be inconsistent with an origin as pingos.

### 5.5. Mud Volcanoes

[25] On Earth, the term “mud volcano” covers a wide range of different features from meter sized cones to domical structures hundreds of meters in size [Kholodov, 2002]. However, terrestrial mud volcanoes are all the result of gas discharge, often accompanied by the explosive eruption, or less violent effusion of soft (i.e., wet) sediments. Terrestrial mud volcanoes also occur within sedimentary basins and the roots of the mud volcanoes are believed to extend to the lowest levels of the sedimentary stack in these basins [Grigor'yants, 2001]. In larger terrestrial mud volcanoes, the active volatile agent is most often methane; however, there are rare occurrences of mud volcanoes that emit CO<sub>2</sub> or nitrogen [Dimitrov, 2002]. On Mars, the driving gas could plausibly be CO<sub>2</sub>, H<sub>2</sub>O, or methane, but CO<sub>2</sub> released from decomposing water-CO<sub>2</sub> or water-CH<sub>4</sub> clathrates might be the most likely [Kargel et al., 2000; Hoffman, 2000]. In the following discussion, some characteristics of subaerial and submarine terrestrial mud volcanoes are described.

[26] The larger terrestrial examples are similar in lateral and vertical dimension to the Martian domes and cones of the Acidalia region. They can have summit depressions of variable size and appear to be most comparable to the cone shaped mud volcanoes described by Kholodov [2002]. Submarine mud volcanoes described from the Gulf of Cadiz have symmetric cone shaped morphologies without summit craters [Somoza et al., 2003]. These features have diameters that range from 0.8 to 2 km and are associated with steeper flanked cones and with rounded craters. While the bulk of the life of a mud volcano involves relatively passive effusion of fluid mud, they also can explode violently if the gas release becomes constricted. There can be secondary and satellite surface vents for a single mud volcano [Dimitrov, 2002], providing an explanation for the multiple pits seen in Figure 3b. The dried, loosely cemented, mud deposits would be a good match to both the albedo and thermal inertia measurements from the Martian domes and cones. Terrestrial mud volcanoes are also found concentrated along subsurface fractures that focus the flow of gas and mud. This matches the observation that the domes and cones in the Acidalia region can be concentrated along possible buried impact crater margins and are sometimes found in chains. Repeated outflow of mud could explain the coarse layering seen in the summit pits of the cones. Effusive mudflows flowing downslope could account for the asymmetric cones shown in Figure 4b.

[27] The difference in morphology in the Acidalia and Cydonia cones and domes could be related to changes in the nature of the sediments and blocks making up the constructs. Cifci and Ergun [2004], in describing the morphology of submarine mud volcanoes, note that when thick mud breccias are erupted, the resulting construct is in the form of a cone with steep flanks, but when the mud breccia is thinned with water, the volcano is low in height with a flatter morphology. This description closely matches the change in morphology from the southern cones to the northern domes. We posit that the change in morphology could be due to a greater abundance of subsurface water

during the mud eruptions that produced the northern domes. Given that the northern domes occur at lower elevations, this hypothesis comports well with a downslope concentration of water.

[28] The volatilization of near surface pockets of clathrates could also produce depressions and a limited effusion of volatiles and sediment leading to the “pancake” features in Figures 3d and 7. Given that ices can be stable at shallower depths further to the north, the bright patches associated with the northern domes might be caused by spontaneous vaporization of very shallowly buried clathrates. Craters on the terrestrial seafloor have been similarly attributed to the explosive decompression of clathrate-hydrates [Solheim and Elverhoi, 1993]. As has been observed with both Mars Exploration Rovers at two very different sites on Mars, the surface layer can be very thin with the result that a minor disturbance (such as pounding or scraping by the airbag landing system) can produce a marked albedo difference [Bell et al., 2004a]. In this instance, the vaporization of shallowly buried clathrates (perhaps at times of low orbital obliquity [Mellon and Jakosky, 1995]) would have displaced the shallow surface veneer of dark sediments with lighter sediments lying beneath. A similar mechanism with a limited (not enough subsurface material removed to form a crater) eruption of subsurface sediments could account for the bright splotches of Figure 3c.

[29] To summarize, there are a number of similarities between terrestrial mud volcanoes and the cones and domes discussed in this paper. The loosely cemented mud mantles of mud volcanoes could account for the observed thermal inertia character of the cones and dome. Repeated eruptions could account for layering seen in craters of some of the Martian cones and dome. Flow of mud downslope could account for the asymmetric aprons in the cones in Figure 4b. Finally, formation processes for mud volcanoes accord well with trends seen in the Acidalia cones and domes. Mud volcanoes occur in sedimentary basins and Acidalia is a basin which, is widely believed to be filled with sediments brought in from the outflow channels. Also, the occurrence of some cones and domes in chains or in concentrations around buried crater margins accords well with the observation that terrestrial mud volcanoes are often concentrated along subsurface fractures.

### 5.6. Springs and Geysers

[30] On Earth, both hot and cold springs can form extensive evaporite deposits around their sources. Hot springs can also erupt water in the form of geysers. The fundamental difference between spring/geyser deposits and mud volcanoes is that the structures are composed primarily of evaporites in the case of springs but primarily clastic sediment in the case of mud volcanoes. The constructs around springs and geysers can have a variety of sizes and shapes, including sizes and shapes similar to the cones and domes seen in the Acidalia region. In their study of clusters of spring mounds in southern Tunisia, Roberts and Mitchell [1987] note that these features can range from 1 to 30 m in height and can achieve diameters of 500 m. Terrestrial spring deposits commonly have pits at their summits. These can be small holes or broad depressions that held water in a surficial basin. The locus of spring

activity can shift with time, producing multiple pits in a single mound. The spring mounds described by *Roberts and Mitchell* [1987] from southern Tunisia are a good morphologic analog to the domes and cones we have observed; albeit with heights at the low end of the range observed for the Acidalia pitted cones. Some of the Tunisian mounds are described as consisting of cemented gypsiferous sand, organic fragments, eolian sand lenses, and “gypsiferous rubble”. Others have a larger component of travertine. Some of the Tunisian mounds have stratigraphy visible in their inner rims (just as some of the pitted cones, such as those in Figures 3b and 4b, have layering visible). Some significant differences can be expected between terrestrial and Martian spring/geyser deposits. On Earth, the dominant mineral is often travertine, a form of calcium carbonate. On Mars, there is little evidence for carbonate deposits, but there is ample evidence for sulfate evaporites [*Suyres et al.*, 2004; *Gendrin et al.*, 2004]. Thus the Martian spring deposits are likely to have a different mineralogy than terrestrial ones. However, either mineralogy would produce an albedo higher than the surrounding basaltic plains. Albedos of the basaltic plains and (presumed) evaporitic outcrops examined by the Opportunity rover at Meridiani Planum are  $0.14 \pm 0.01$  and  $0.25 \pm 0.06$  [*Bell et al.*, 2004b]. Thus the albedos of the evaporites observed at Meridiani are brighter than the observed albedos of the southern cones and northern domes (Table 2). Terrestrial spring mounds contain clastic sediments so it is likely that analogous Martian spring mounds could incorporate low-albedo basaltic clasts that would result in a lower albedo for the spring mounds than for the areally extensive Meridiani evaporites. Some terrestrial spring deposits are described in the literature as “porous” [e.g., *Guidry and Chafetz*, 2003]. Martian spring deposits might be even more porous. The thinner atmosphere on Mars should have a significant effect on surface evaporation. Not only will liquid water evaporate quickly, the uppermost layer can boil vigorously. This could lead to relatively porous deposits on Mars as compared to the Earth. Such porosity could help explain the thermal properties of the cones and domes on Mars. The erosion, through eolian activity, of an outer, highly porous layer could explain the more eroded appearance and seemingly higher thermal inertia of some of the southern cones compared to the northern domes.

### 5.7. Relevance of Pitted Cone Origin Modes for Models of the Northern Plains

[31] The set of possible origins addressed in the preceding discussion have implications for the history of the Acidalia Planitia region, and for the VBF which covers much of northern Acidalia. The interpretation of the pitted cones as mud volcanoes accords well with the interpretation of the VBF as sedimentary residue from the outflow channels to the south. In effect, Acidalia is a sedimentary basin under this interpretation. On Earth, mud volcanoes are associated with sedimentary basins; thus the presence of mud volcanoes accords well with this interpretation. It is unknown what the primary gas associated with this putative mud volcanism was. On Earth, methane is the primary gas associated with mud volcanism. On Mars, the primary gas could have been  $\text{CO}_2$ , although recent observations of methane in the Martian atmosphere [*Formisano et al.*,

2004; *Krasnopolsky et al.*, 2004] allow for the possibility that methane might also have played a role in the formation of the pitted cones discussed in this paper.

[32] The other preferred interpretation, that the pitted cones might be dome to cone shaped spring deposits, would be evidence of a formerly active subsurface hydrological system in Acidalia. It would also require periods after the deposition of the VBF (post early Amazonian) for the climate to have been warm enough to allow water (likely brine-saturated water) to flow to the surface and evaporate away to leave the evaporitic spring deposits.

## 6. Summary and Conclusions

[33] Pitted cones in Acidalia Planitia and Cydonia Mensae were studied using MOC NA imagery, THEMIS MWIR and VNIR data, and a TES-derived map of thermal inertia [*Mellon et al.*, 2002]. The pitted cones observed in Acidalia and Cydonia can be separated into two major groups: those that lie predominantly south of  $40.5^\circ\text{N}$  latitude tend to have a more cone-like morphology; those that occur predominantly north of that latitude tend to have a more dome-like morphology. The northern domes are higher in albedo than the surrounding plains and also have lower apparent thermal inertias than the surrounding plains. The southern cones have albedos and thermal inertias that are commensurate with the surrounding plains. The thermal inertia values of the pitted cones and domes are between those of basaltic fine dust and sand while that of the surrounding plains are closer to that of basaltic sand.

[34] After examining various possible formation processes for the cones and domes of the northern plains, we have reached several general conclusions. Largely on the basis of the absence of associated volcanic flow features, we consider a cinder cone or rootless cone origin for the pitted cones to be unlikely. While we cannot completely eliminate a phreatomagmatic origin, neither can we find any compelling evidence for such an origin. Similarly, the observations appear to be generally inconsistent with an origin as pingos. Instead, we find the visible and thermal observations are most consistent with these cones and domes having formed via mud volcanism, geysers, and/or springs. It is possible that some combination of these processes acted to form the observed cones and domes. The process of mud volcanism, by itself, could potentially account for the observed differences in the morphology of the cones in the southern and northern portion of the study area. When copious amounts of water are included in a mud volcano eruption, the erupted sediments are thinned by the water and the flanks of the resulting structure are not as steep. In a dryer mud volcano eruption, the erupted mud breccia is thicker and can form a cone with steep flanks [*Cifci and Ergun*, 2004]. The change in morphology from south to north could thus indicate that more water was available at the time and locations of the eruptive processes that formed the northern domes. Thus an origin of the northern plains cones and domes involving some form of mud volcanism is compelling.

[35] The prospect that some of the pitted cones might be the Martian equivalent of terrestrial spring mounds is also intriguing. Morphologically, they seem to be a good match to spring mounds that occur in southern Tunisia [*Roberts and Mitchell*, 1987]. Assuming that the evaporitic materials

are porous, as is often the case with terrestrial spring deposits, these materials could also account for the observed albedo and thermal characteristics. Spring deposits can form a variety of landforms and some combination of changes in temperature related to differences in latitude, changes in atmospheric pressure related to differences in elevation, and changes in the nature of the near surface geology could account for the differences in morphology between the northern domes and the southern cones.

[36] Origin by mud volcanism, eruption of geysers and/or springs, or some combination of these processes could account for the observed occurrences of northern domes and southern cones. While we cannot distinguish between or among these processes with the data available currently, we conclude that the formation of both cones and domes most likely involved the presence of water, but the exact role of liquid water is still not clear. Either the mud volcanism or spring processes are supportive of the idea that large amounts of water were once present across much of the northern plains of Mars. However, we cannot place any strong constraints on whether this water was in the form of groundwater (either mobile or immobile), intermittent seas, or a long-lived ocean. Analyses of new, high spatial-resolution imaging in conjunction with hyperspectral observations, such as will be available from the HiRISE [McEwen *et al.*, 2002] and CRISM [Murchie *et al.*, 2002] instruments on the upcoming Mars Reconnaissance Orbiter, will be essential for distinguishing between the different remaining hypotheses for the formation of these intriguing features. In particular, the CRISM data could be used to readily prove or disprove the spring deposit hypothesis since such features are formed from evaporite minerals (on Earth, largely travertine, but on Mars perhaps primarily sulfate minerals such as gypsum and kieserite) with distinctive spectral signatures.

[37] **Acknowledgments.** This research was funded under the NASA Office of Space Science Mars Data Analysis Program grant number NAG5-10577. We thank Catherine Weitz of the Planetary Science Institute and reviewers Sarah Fagents, Peter Lanagan and an anonymous reviewer for helpful reviews.

## References

- Allen, C. C. (1979), Volcano/ice interactions on Mars, *J. Geophys. Res.*, **84**, 8048–8059.
- Baker, V. R., R. G. Strom, V. C. Gulick, J. S. Kargel, G. Komatsu, and V. S. Kale (1991), Ancient oceans, ice sheets, and the hydrological cycle on Mars, *Nature*, **352**, 589–594.
- Bandfield, J. L. (2002), Global mineral distribution on Mars, *J. Geophys. Res.*, **107**(E6), 5042, doi:10.1029/2001JE001510.
- Bandfield, J. L. (2003), Martian global surface mineralogy from the Thermal Emission Spectrometer: Surface emissivity, mineral map, and spectral endmember data products, in *Sixth International Conference on Mars* [CD-ROM], abstract 3052, Lunar and Planet. Inst., Houston, Tex.
- Bandfield, J. L., V. E. Hamilton, and P. R. Christensen (2000), A global view of Martian surface compositions from MGS-TES, *Science*, **287**, 1626–1630.
- Becker, T., E. Eliason, K. Becker, and USGS Astrogeology Team (2004), ISIS Workshop: Processing for MGS/MOC imaging, U.S. Geol. Surv., Flagstaff, Ariz. (Available at [http://isis.astrogeology.usgs.gov/Isis2/gifs/mgs\\_moc.pdf](http://isis.astrogeology.usgs.gov/Isis2/gifs/mgs_moc.pdf))
- Bell, J. F., III, *et al.* (2004a), Pancam multispectral imaging results from the Spirit rover at Gusev Crater, *Science*, **305**, 800–806.
- Bell, J. F., III, *et al.* (2004b), Pancam multispectral imaging results from the Opportunity rover at Meridiani Planum, *Science*, **306**, 1703–1709.
- Bruno, B. C., S. A. Fagents, T. Thordarson, S. M. Baloga, and E. Pilger (2004), Clustering within rootless cone groups on Iceland and Mars: Effect of nonrandom processes, *J. Geophys. Res.*, **109**, E07009, doi:10.1029/2004JE002273.
- Christensen, P. R., *et al.* (2004), The Thermal Emission Imaging System (THEMIS) for the Mars 2001 Odyssey Mission, *Space Sci. Rev.*, **110**, 85–130.
- Cifci, G., and M. Ergun (2004), Image characteristics of the Mediterranean Sea and the Black Sea mud volcanoes and sea bed features, paper presented at Second Balkan Geophysical Congress and Exhibition, Balkan Geophys. Soc., Bucharest, Romania. (Available at <http://www.balkangeophysoc.org/menu/congresses/oral/12-13-04-1-gunay-cifci.PDF>)
- Clifford, S. M., and T. J. Parker (2001), The evolution of the Martian hydrosphere: Implications for the fate of a primordial ocean and the current state of the northern plains, *Icarus*, **154**, 40–79.
- Crumpler, L. S. (2003), Physical characteristics, geologic setting, and possible formation processes of spring deposits on Mars based on terrestrial analogs, in *Sixth International Conference on Mars* [CD-ROM], abstract 3228, Lunar and Planet. Inst., Houston, Tex.
- DeGans, W. (1988), Pingo scars and their identification, in *Advances in Periglacial Geomorphology*, edited by M. J. Clark, pp. 299–322, John Wiley, Hoboken, N. J.
- Dimitrov, L. I. (2002), Mud volcanoes—The most important pathway for degassing deeply buried sediments, *Earth Sci. Rev.*, **59**, 49–76.
- Eliason, E. (1997), Production of digital image models (DIMs) using ISIS, *Lunar Planet. Sci.*, **XVIII**, abstract 331.
- Fagents, S. A., P. Lanagan, and R. Greeley (2002), Rootless cones on Mars: A consequence of lava-ground ice interaction, in *Volcano-Ice Interaction on Earth and Mars*, edited by J. L. Smellie and M. G. Chapman, *Geol. Soc. Spec. Publ.*, **202**, 295–317.
- Farrand, W. H., and L. R. Gaddis (2003a), Analysis of MGS TES data over Acidalia Planitia and Cydonia Mensae: Compositional evidence for hydrovolcanic activity, *Lunar Planet. Sci.*, **XXXIV**, abstract 1601.
- Farrand, W. H., and L. R. Gaddis (2003b), THEMIS Observations of pitted cones in Acidalia Planitia and Cydonia Mensae, in *Sixth International Conference on Mars*, abstract 3094, Lunar and Planet. Inst., Houston, Tex.
- Farrand, W. H., and R. B. Singer (1992), Alteration of hydrovolcanic basaltic ash: Observations with visible and near-infrared spectrometry, *J. Geophys. Res.*, **97**, 17,393–17,408.
- Ferguson, R. L., and P. R. Christensen (2003), Thermal inertia using THEMIS infrared data, *Lunar Planet. Sci.*, **XXXIV**, abstract 1785.
- Formisano, V., S. Atreya, T. Encrenaz, N. Ignatiev, and M. Giuranna (2004), Detection of methane in the atmosphere of Mars, *Science*, **306**, 1758–1761.
- Frey, H. M., and M. Jarosewich (1982), Subkilometer Martian volcanoes: Properties and possible terrestrial analogs, *J. Geophys. Res.*, **87**, 9867–9879.
- Frey, H. M., B. L. Lowry, and S. A. Chase (1979), Pseudocraters on Mars, *J. Geophys. Res.*, **84**, 8075–8086.
- Gaddis, L., *et al.* (1997), An overview of the Integrated Software for Imaging Spectrometers (ISIS), *Lunar Planet. Sci.*, **XVIII**, abstract 387.
- Geissler, P. E. (2005), Three decades of Martian surface changes, *J. Geophys. Res.*, **110**, E02001, doi:10.1029/2004JE002345.
- Geissler, P. E., R. B. Singer, and B. K. Lucchitta (1990), Dark materials in Valles Marineris: Indications of the style of volcanism and magmatism on Mars, *J. Geophys. Res.*, **95**, 14,399–14,413.
- Gendrin, A., J.-P. Bibring, B. Gondet, Y. Langevin, N. Mangold, J. F. Mustard, F. Poulet, and C. Quantin (2004), Identification of sulfate deposits on Mars by OMEGA/Mars Express, paper presented at Second Conference on Early Mars, Lunar and Planet. Inst., Jackson Hole, Wyo.
- Gillespie, A. R., A. B. Kahle, and R. E. Walker (1986), Color enhancement of highly correlated images: I. Decorrelation and HSI contrast stretches, *Remote Sens. Environ.*, **20**, 209–235.
- Greeley, R., and S. A. Fagents (2001), Icelandic pseudocraters as analogs to some volcanic cones on Mars, *J. Geophys. Res.*, **106**, 20,527–20,546.
- Grigor'yants, B. V. (2001), Mud volcanism as a source of geological information, *Geotectonics*, **35**, 207–216.
- Guidry, S. A., and H. S. Chafetz (2003), Depositional facies and diagenetic alteration in a relict siliceous hot-spring accumulation: Examples from Yellowstone National Park, U.S.A., *J. Sediment. Res.*, **73**, 806–823.
- Gurney, S. D. (1998), Aspects of the genesis and geomorphology of pingos: Perennial permafrost mounds, *Progr. Phys. Geogr.*, **22**, 307–324.
- Hare, T. M., and K. L. Tanaka (2004), Expansion in geographic information services for PIGWAD, *Lunar Planet. Sci.*, **XXXV**, abstract 1765.
- Head, J. W., H. Hiesinger, M. A. Ivanov, M. A. Kreslavsky, S. Pratt, and B. J. Thomson (1999), Possible ancient oceans on Mars: Evidence from Mars Orbiter Laser Altimeter data, *Science*, **286**, 2137–2143.
- Hoffman, N. (2000), White Mars: A new model for Mars' surface and atmosphere based on CO<sub>2</sub>, *Icarus*, **146**, 326–342.
- Jöns, H.-P. (1985), Late sedimentation and late sediments in the northern lowlands of Mars, *Lunar Planet. Sci.*, **XVI**, 414–415.
- Jöns, H.-P. (1986), Arcuate ground undulations, gelifluxion-like features and “front tori” in the northern lowlands on Mars—What do they indicate?, *Lunar Planet. Sci.*, **XVII**, 404–405.

- Kargel, J. S., K. L. Tanaka, V. R. Baker, G. Komatsu, and D. R. MacAyeal (2000), Formation and dissociation of clathrate hydrates on Mars: Polar caps, northern plains, and highlands, *Lunar Planet. Sci.*, XXXI, abstract 1891.
- Keszthelyi, L. (1994), Calculated effect of vesicles on the thermal properties of cooling basaltic lava flows, *J. Volcanol. Geotherm. Res.*, 63, 257–266.
- Kholodov, V. N. (2002), Mud volcanoes, their distribution, regularities, and genesis: Communication 1. Mud volcanic provinces and morphology of mud volcanoes, *Lithol. Miner. Resour.*, 27, 197–209.
- Krasnopolsky, V. A., J. P. Maillard, and T. C. Owen (2004), Detection of methane in the Martian atmosphere: Evidence for life?, *Icarus*, 172, 537–547.
- Kreslavsky, M. A., and J. W. Head (2002), Fate of outflow channel effluents in the northern lowlands of Mars: The Vastitas Borealis Formation as a sublimation residue from frozen ponded bodies of water, *J. Geophys. Res.*, 107(E12), 5121, doi:10.1029/2001JE001831.
- Lanagan, P. D., A. S. McEwen, L. P. Keszthelyi, and T. Thordarson (2001), Rootless cones on Mars indicating the presence of shallow equatorial ground ice in recent times, *Geophys. Res. Lett.*, 28, 2365–2367.
- Lucchitta, B. K. (1981), Mars and Earth: Comparison of cold-climate features, *Icarus*, 45, 264–303.
- Mackay, J. R. (1973), The growth of pingos, western Arctic coast, Canada, *Can. J. Earth Sci.*, 10, 979–1004.
- MacKay, J. R. (1998), Pingo growth and collapse, Tuktoyaktuk Peninsula area, western arctic coast, Canada: A long-term field study, *Geogr. Phys. Quat.*, 52, 1–53.
- McEwen, A. S., et al. (2002), HiRISE: The High Resolution Imaging Science Experiment for the Mars Reconnaissance Orbiter, *Lunar Planet. Sci.*, XXXIII, abstract 1163.
- McGill, G. E. (2002), The small domes and pits of Cydonia Mensae and adjacent Acidalia Planitia, Mars: Implications for the role of near surface water or ice, *Lunar Planet. Sci.*, XXXIII, abstract 1126.
- McGill, G. E., and L. S. Hills (1992), Origin of giant Martian polygons, *J. Geophys. Res.*, 97, 2633–2647.
- Mellon, M. T. (2001), Thermal inertia and rock abundance, paper presented at Thermal Emission Spectrometer workshop, Ariz. State Univ., Tempe, Ariz.
- Mellon, M. T., and B. M. Jakosky (1995), The distribution and behavior of Martian ground ice during past and present epochs, *J. Geophys. Res.*, 100, 11,781–11,799.
- Mellon, M. T., K. A. Kretke, M. D. Smith, and S. M. Pelkey (2002), A global map of thermal inertia from Mars Global Surveyor mapping-mission, *Lunar Planet. Sci.*, XXXIII, abstract 1416.
- Morrissey, M. M., and T. Thordarson (1991), Origins and occurrences of pseudocrater fields in S. Iceland, *Eos Trans. AGU*, 72, 556.
- Murchie, S., et al. (2002), CRISM: Compact Reconnaissance Imaging Spectrometer for Mars on the Mars Reconnaissance Orbiter, *Lunar Planet. Sci.*, XXXIII, abstract 1697.
- Parker, T. J., R. S. Saunders, and D. M. Schneeberger (1989), Transitional morphology in West Deuteronilus Mensae, Mars: Implications for modification of the Lowland/Upland boundary, *Icarus*, 82, 111–145.
- Parker, T. J., D. S. Gorsline, R. S. Saunders, D. C. Pieri, and D. M. Schneeberger (1993), Coastal geomorphology of the Martian northern plains, *J. Geophys. Res.*, 98, 11,061–11,078.
- Pike, R. J., and G. D. Clow (1981), Revised classification of terrestrial volcanoes and catalog of topographic dimensions, with new results on edifice volume, *U.S. Geol. Surv. Open File Rep.*, 81-1038, 40 pp.
- Pissart, A. (1988), Pingos: An overview of the present state of knowledge, in *Advances in Periglacial Geomorphology*, edited by M. J. Clark, pp. 279–297, John Wiley, Hoboken, N. J.
- Ramsey, M. S., and P. R. Christensen (1998), Mineral abundance determination: Quantitative deconvolution of thermal emission spectra, *J. Geophys. Res.*, 103, 577–596.
- Roberts, C. R., and C. W. Mitchell (1987), Spring mounds in southern Tunisia, in *Desert Sediments: Ancient and Modern*, edited by L. Frostick and I. Reid, *Geol. Soc. Spec. Publ.*, 35, 321–334.
- Scott, D. H., and K. L. Tanaka (1986), Geologic map of the western equatorial region of Mars, *U.S. Geol. Surv. Geol. Invest. Ser., Map I-1802A*.
- Solheim, A., and A. Elverhoi (1993), Gas-related sea floor craters in the Barents Sea, *Geo Mar. Lett.*, 13, 235–243.
- Somoza, L., et al. (2003), Seabed morphology and hydrocarbon seepage in the Gulf of Cadiz mud volcano area: Acoustic imagery, multibeam and ultra-high resolution seismic data, *Mar. Geol.*, 195, 153–176.
- Squyres, S. W., et al. (2004), In-situ evidence for an ancient aqueous environment on Mars, *Science*, 306, 1709–1714.
- Tanaka, K. L. (1997), Sedimentary history and mass flow structures of Chryse and Acidalia Planitiae, Mars, *J. Geophys. Res.*, 102, 4131–4150.
- Tanaka, K. L., W. B. Banerdt, J. S. Kargel, and N. Hoffman (2001), Huge, CO<sub>2</sub>-charged debris-flow deposit and tectonic sagging in the northern plains of Mars, *Geology*, 29, 427–430.
- Tanaka, K. L., J. A. Skinner Jr., T. M. Hare, T. Joyal, and A. Wenker (2003), Resurfacing history of the northern plains of Mars based on geologic mapping of Mars Global Surveyor data, *J. Geophys. Res.*, 108(E4), 8043, doi:10.1029/2002JE001908.
- Thorarinsson, S. (1953), The crater groups in Iceland, *Bull. Volcanol.*, 14, 3–44.
- Torson, J. M., and K. J. Becker (1997), ISIS—A software architecture for processing planetary images, *Lunar Planet. Sci.*, XXVIII, abstract 1443.
- Wilson, L., and J. W. Head (1983), A comparison of volcanic eruption processes on Earth, Moon, Mars, Io, and Venus, *Nature*, 302, 663–669.
- Wohletz, K. M., and M. F. Sheridan (1983), Hydrovolcanic explosions II. Evolution of basaltic tuff rings and tuff cones, *Am. J. Sci.*, 283, 385–413.
- Wood, C. A. (1979), Monogenetic volcanoes of the terrestrial planets, *Proc. Lunar Planet. Sci. Conf. 10th*, 2815–2840.
- Wyatt, M. B., and H. Y. McSween (2002), Spectral evidence for weathered basalt as an alternative to andesite in the northern lowlands of Mars, *Nature*, 417, 263–266.
- Zimbelman, J. R. (1986), The role of porosity in thermal inertia variations on basaltic lava, *Icarus*, 68, 366–369.

---

W. H. Farrand, Space Science Institute, 4750 Walnut Street, Suite 205, Boulder, CO 80301, USA. (farrand@spacescience.org)  
 L. R. Gaddis and L. Keszthelyi, Astrogeology Team, U.S. Geological Survey, 2255 North Gemini Drive, Flagstaff, AZ 86001, USA.